Structural XAFS Investigation of Eu2+ and Sr2+ Poly(amino carboxylates): Consequences for Water Exchange Rates on MRI-Relevant Complexes

ARTICLE *in* THE JOURNAL OF PHYSICAL CHEMISTRY A · FEBRUARY 2003

Impact Factor: 2.69 · DOI: 10.1021/jp0267510 · Source: OAI

5 AUTHORS, INCLUDING:

Lothar Helm
École Polytechnique Fédérale de Lausanne
240 PUBLICATIONS **7,748** CITATIONS
SEE PROFILE

Juris Purans
University of Latvia
221 PUBLICATIONS **1,849** CITATIONS
SEE PROFILE

André E Merbach
École Polytechnique Fédérale de Lausanne
463 PUBLICATIONS **14,063** CITATIONS
SEE PROFILE

Structural XAFS Investigation of Eu^{2+} and Sr^{2+} Poly(amino carboxylates): Consequences for Water Exchange Rates on MRI-Relevant Complexes

Gilles Moreau,[†] László Burai,[†] Lothar Helm,[†] Juris Purans,[†,‡] and André E. Merbach*,[†]

Institute of Molecular and Biological Chemistry, Swiss Federal Institute of Technology Lausanne, EPFL-BCH, CH-1015 Lausanne, Switzerland, and Institute of Solid State Physics, Kengaraga Str. 8, LV-1063 Riga, Latvia

Received: August 13, 2002; In Final Form: November 26, 2002

The structure of the Eu^{2+} and Sr^{2+} $DOTA^{4-}$ (1,4,7,10-tetraazacyclododecane-1,4,7,10-tertraacetate), $DTPA^{5-}$ (diethylenetriamine-*N*,*N*,*N*′,*N*″,*N*″-pentaacetate), and $ODDA^{2-}$ (1,4,10,13-tetraoxa-7,16-diazacyclooctadecane-7,16-diacetate) complexes were characterized using XAFS in the solid state and in aqueous solution. The results show the structural similarity between the highly paramagnetic and MRI-relevant Eu^{2+} poly(amino carboxylate) complexes with their diamagnetic Sr^{2+} homologues in each state as well as the overall conservation of the solid-state structure in aqueous solution. The $DOTA^{4-}$ ligand adopts a twisted-square antiprism conformation in aqueous solution to accommodate the large Eu^{2+} and Sr^{2+} ions, leading to metal ion-to-coordinated water distances 0.2 Å longer in the $[M^{II}(DOTA)(H_2O)]^{2-}$ complexes than in the $[M^{II}(DTPA)(H_2O)]^{3-}$ complexes ($M^{II} = Eu^{2+}$, Sr^{2+}). The different structures adopted by the complexes in aqueous solution were found to be responsible for their different water exchange mechanisms: changing from D ($DTPA^{5-}$, $DOTA^{4-}$) for Gd^{3+} to I_d ($DTPA^{5-}$), I ($DOTA^{4-}$), and I_a ($ODDA^{2-}$) for the Eu^{2+} complexes. Finally, a lower charge density and substantially longer $M-O_w$ distances for the Eu^{2+} ion explain the 3 orders of magnitude higher water exchange rates observed for the Eu^{2+} poly(amino carboxylates) over the corresponding Gd^{3+} complexes. Such high water exchange rates could be valuable in designing more efficient responsive contrast agents for magnetic resonance imaging.

Introduction

Over the past two decades, Gd^{3+} poly(amino carboxylate) complexes have become widely used as contrast agents in medical diagnostics using magnetic resonance imaging (MRI).[1] Eu^{2+} (1.30 Å ionic radius[2] for nine coordination) is isoelectronic to Gd^{3+} (1.11 Å) and shows similar magnetic properties. The high magnetic moment of both ions ($S = {}^7/_2$), associated with relatively slow electron-spin relaxation rates, makes them an ideal choice for nuclear magnetic relaxation enhancement,[3,4] a highly regarded property in contrast agents for medical MRI.[1]

The characterization of Eu^{2+} complexes has been hindered by their poor stability in aqueous solution[5] because they react quickly with oxygen and more slowly with water.[6] Moreover, Eu^{2+} is intermediate in size between the chemically stable and diamagnetic Ca^{2+} and Sr^{2+} (1.18 and 1.31 Å ionic radii,[2] respectively, for nine coordination) and exhibits similar coordination chemistry.[7] Thus, the Sr^{2+} ion can be used as a chemically stable model for the Eu^{2+} complexes. Reciprocally, investigations of paramagnetic Eu^{2+} complexes using electron spin resonance (ESR) or nuclear magnetic resonance (NMR) relaxation give access to the water exchange rates and mechanism of the homologous Sr^{2+} complexes.

Recently it was demonstrated that careful preparation allows the production of samples that are stable for a few hours,[8] which makes Eu^{2+} complexes of potential interest as MRI contrasting agents. Furthermore, the reaction of Eu^{2+} poly(amino carboxylate) complexes with oxygen or water could potentially be exploited in the clinic to produce responsive or "smart" contrast agents.[4] MRI research tends toward specific compounds that are able to produce an image depending on the physicochemical properties of their biological environment.

SCHEME 1

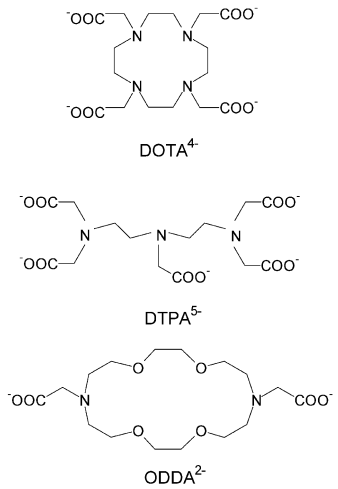

We recently studied the dynamic properties of the Eu^{2+} DOTA,[4−] $DTPA^{5-}$, and $ODDA^{2-}$ complexes (Scheme 1) in aqueous solution.[9−11] $DOTA^{4-}$ (1,4,7,10-tetraazacyclododecane-1,4,7,10-tetraacetate) and $DTPA^{5-}$ (diethylenetriamine-*N*,*N*,*N*′,-*N*″,*N*″-pentaacetate) are among the most commonly used ligands for MRI contrast agents (Dotarem, Magnevist) and are used as building blocks in more specific contrast agents, and $ODDA^{2-}$ (1,4,10,13-tetraoxa-7,16-diazacyclooctadecane-7,16-diacetate) forms the most redox-stable Eu^{2+} poly(amino carboxylate) complex studied so far. Until now, however, the only structural

* To whom correspondence should be addressed. E-mail: andre.merbach@epfl.ch. Phone: +41-21-693-98-71. Fax: +41-21-693-98-75.
† Swiss Federal Institute of Technology Lausanne.
‡ Institute of Solid State Physics.

10.1021/jp0267510 CCC: $25.00
Published on Web 01/01/2003

information available for these Eu^{2+} complexes was the crystal structure of $[Eu(DTPA)(H_2O)][C(NH_2)_3]_3$.[10] Because this compound is quasi-isostructural with the corresponding Sr^{2+} complex, the isostructurality was presupposed for the other Eu^{2+} and Sr^{2+} poly(amino carboxylate) complexes, which have not been crystallized with the Eu^{2+} ion. Additionally, structural investigations have been performed on the Gd^{3+} $DOTA^{4-}$ and $DTPA^{5-}$ complexes using the X-ray absorption fine structure (XAFS) technique, which shows that the overall structure was retained in aqueous solution.[12] It was consequently supposed, given the high complexing properties of these poly(amino carboxylate) ligands, that the coordination polyhedron geometry of the Eu^{2+} ion was also retained in aqueous solution.

In the present work, the XAFS technique is used to characterize and compare the Eu^{2+} and Sr^{2+} DOTA,$^{4-}$ $DTPA^{5-}$, and $ODDA^{2-}$ complexes in the solid state and in solution. The experimental Eu^{2+} L_3-edge as well as the Sr^{2+} K-edge XAFS spectra have been measured, analyzed, and compared using a theoretical approach[13] combined with efficient analysis techniques.[14−16] Finally, the water exchange reaction rates and mechanisms of these Eu^{2+} and Sr^{2+} poly(amino carboxylate) complexes are discussed on a structural basis.

Experimental Section

Chemicals. H_4DOTA was purchased from Strem Chemicals, H_5DTPA and $[C(NH_2)_3]_2CO_3$ were purchased from Fluka, H_2ODDA was purchased from Acros Organics, and 98% CF_3SO_3H (triflic acid) was purchased from Aldrich Chemicals. All commercial compounds were used as received. $[Eu(H_2O)_9](O_3SCF_3)_3$ was prepared as described in the literature.[17]

The compounds $[Eu(DOTA)(H_2O)][C(NH_2)_3]_2$,[11] $[Eu(DTPA)(H_2O)][C(NH_2)_3]_3$,[10] $[Sr(DOTA)(H_2O)][C(NH_2)_3]_2$,[11] $[Sr(DTPA)(H_2O)][C(NH_2)_3]_3$,[10] and Sr(ODDA)[10] were obtained from $[Eu(H_2O)_9](O_3SCF_3)_3$ and analytical grade $SrCO_3$ following literature procedures. The solid Eu(ODDA) was obtained by the evaporation of an electrochemically reduced solution of the corresponding Eu^{3+} complex.[10] Crystals were not obtained by evaporation, and the resulting solid material contains about 10% NaO_3SCF_3.

Preparation of the Samples. Solutions of 0.2 M $[Eu(DOTA)(H_2O)]Na_2$, 0.1 M $[Eu(DTPA)(H_2O)]Na_3$, 0.1 M $[Eu(ODDA)(H_2O)]$, 0.2 M $[Sr(DOTA)(H_2O)]Na_2$, 0.1 M $[Sr(DTPA)(H_2O)]Na_3$, and 0.1 M $[Sr(ODDA)(H_2O)]$ were obtained by literature procedures.[9−11] The solid guanidinium samples were finely ground and mechanically mixed with cellulose powder to give pressed pellets with a thickness chosen to obtain an absorption jump value of about 1. All of the Eu^{2+} solid compounds and solutions were prepared, handled, and stored under the oxygen-free nitrogen atmosphere of a glovebox to avoid oxidation.

Calculations of Surface Electrostatic Potentials. The electrostatic potentials on the Sr^{2+} and Gd^{3+} complexes with $DOTA^{4-}$ and $DTPA^{5-}$ ligands and on the Sr(ODDA) complex were described by calculations of their partial atomic charges using the Merz−Kollman method[18] as implemented in the Gaussian 98 package[19] and based on the X-ray crystal structures of the complexes.[10,11,20,21] This method outputs atomic charges by fitting them to the electrostatic potential at a fixed distance through a dielectric medium, leading to a good representation of the electrostatic potential at the molecular surface. In the solid-state structure of the Sr^{2+} poly(amino carboxylate) complexes, the position of the protons of the coordinated water molecule is undetermined. Thus, for the calculations, the coordinated water molecule was replaced by an oxygen atom in all Sr^{2+} and Gd^{3+} complexes. For the Sr^{2+} complexes, calculations were performed at the LANL2DZ level (Sr, H, C, N, O), and for the Gd^{3+} complexes, calculations were performed at the 6-31G** level (H, C, N, O), with pseudopotentials by Dolg and Stoll[22] accounting for relativistic corrections in the treatment of the Gd^{3+} core electrons. The electrostatic potentials were plotted on the electronic density maps obtained from the Gaussian 98 outputs using Molekel software,[23] version 4.2, with a cutoff value of 0.012 that is identical for all complexes.

XAFS Measurements. XAFS measurements were performed at the LURE synchrotron radiation facility (Orsay, France) on the DCI D21 (XAS 2) beam line. The positron-beam energy and average current were 1.85 GeV and 320 to 250 mA, respectively. The XAFS spectra of the Eu L_3-edge (6976 eV; 6900−7650 eV scans) and Sr K-edge (16105 eV; 16 000−17 000 eV scans) were measured in transmission mode. The synchrotron radiation was monochromatized using the Si(311) double-crystal monochromator, and in the case of the Eu L_3-edge, harmonic rejection was achieved using dedicated mirrors. The experimental spectra were measured using two ionization chambers (filled with air for Eu and with Ar for Sr measurements) with a count rate of 2 s per point, an energy resolution of 1 or 2 eV, a 0.5 or 1 eV step in the X-ray absorption near-edge structure (XANES) region, and a 1 or 2 eV step in the extended X-ray absorption fine structure (EXAFS) region for the Eu L_3-edge and the Sr K-edge, respectively. A multipurpose X-ray absorption cell[24] was used for the in situ XAFS measurements of sealed, oxygen, and water-free solutions. The measurements were carried out at optical lengths of 1−1.5 mm for Eu and 4−8 mm for Sr, resulting in values of the absorption jump of about 0.5 (white-line amplitude about 2) for Eu and about 1 for Sr. All samples were measured at room temperature (20−25 °C), and at least three complete and identical XAFS scans were collected for each.

Data Analysis. The experimental data were analyzed by implementing a simple constraints refinement based on the crystallographic data and lattice dynamics.[25] Because the coordination polyhedron in the characterized complexes is known (at least in the solid state), only integer values of the occupation numbers were considered, and all atoms of a similar type at similar distances (participating in the same subshell) were attributed the same DW factor, as described previously.[12,26]

Low-symmetry crystalline complexes such as $[Eu(DTPA)(H_2O)]^{3-}$ and $[Eu(DOTA)(H_2O)]^{2-}$ contain many distances in one subshell, thus the fitted Debye−Waller (DW) factors (C_2) include both the static and the dynamic contributions. The experimental XAFS data were treated using the EDA software package,[27] as in the study of the Eu^{2+} and Sr^{2+} ions in water[8] and in nonaqueous solutions.[28] The obtained XAFS spectra, $\chi(E)$, were converted to the *k*-space of the photoelectron wavevector, defined as $k = \sqrt{(2m/\hbar)(E-E_0)}$, where $(E - E_0)$ is the measured photoelectron kinetic energy. The experimental high-energy part of the XAFS spectra $\chi(k)$ (called EXAFS) of both the Eu^{2+} and Sr^{2+} complexes (Figures 1 and 2) was multiplied by a factor of k^3 or k^4 (see Table S1 in Supporting Information for experimental details) to compensate for the decrease in amplitude with increasing wavevector value. A k^4 instead of k^3 factor was occasionally needed (see Results section) to allow a precise single-out of the first shell of scatterers' contribution to the experimental EXAFS spectrum.

The experimental EXAFS spectra were Fourier transformed (FT) with a Kaiser−Bessel window in the 0−12 $Å^{-1}$ range for Eu and the 0−15 $Å^{-1}$ range for Sr (Figures 3 and 4). The first-shell EXAFS contributions were singled out by a back FT

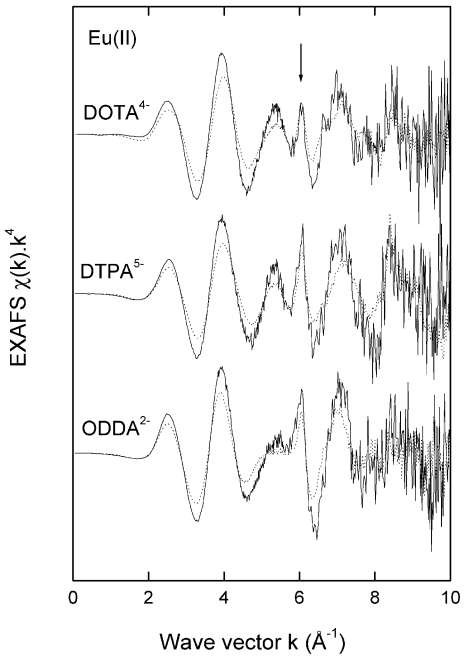

Figure 1. Experimental $\chi(k)k^4$ XAFS spectra of the Eu^{2+} $DOTA^{4-}$, $DTPA^{5-}$, and $ODDA^{2-}$ complexes in the solid state (••) and in solution (—).

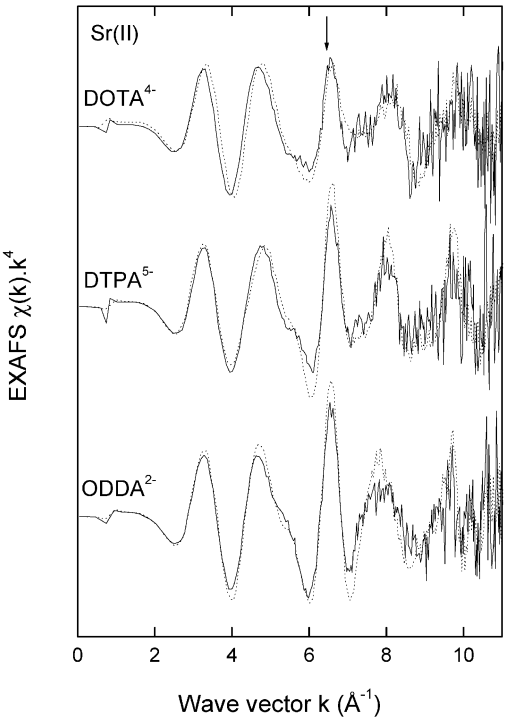

Figure 2. Experimental $\chi(k)k^4$ XAFS spectra of the Sr^{2+} $DOTA^{4-}$, $DTPA^{5-}$, and $ODDA^{2-}$ complexes in the solid state (••) and in solution (—).

procedure in the approximate 1.2−2.6 Å range (see Table S1 for experimental details) for both Eu^{2+} and Sr^{2+}. The FTs were not corrected for a photoelectron phase shift, as all peaks originate from different contributions with different photoelectron phase shifts. Therefore, the peak positions in Figures 3 and 4, as well as the back FT windows (Table S1), differ by about 0.5 Å from the true values obtained during the EXAFS fitting procedure.

The first-shell EXAFS spectra were fitted using standard harmonic two- or three-shell models[29] in which the distribution

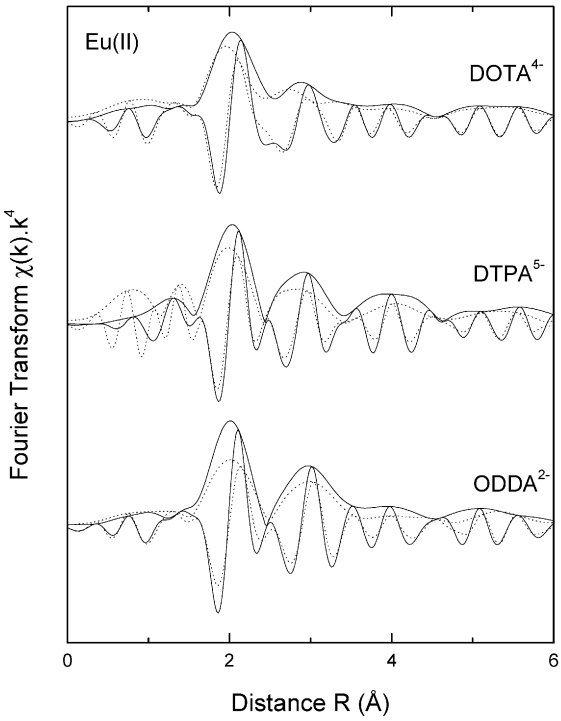

Figure 3. Fourier transforms (modulus and imaginary parts) of the experimental XAFS $\chi(k)k^4$ spectra of the Eu^{2+} $DOTA^{4-}$, $DTPA^{5-}$, and $ODDA^{2-}$ complexes in the solid state (••) and in solution (—).

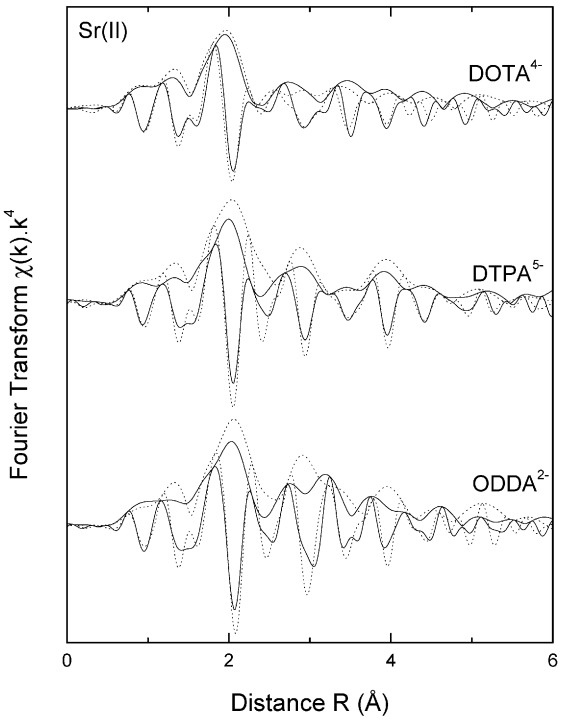

Figure 4. Fourier transforms (modulus and imaginary parts) of the experimental XAFS $\chi(k)k^4$ spectra of the Sr^{2+} $DOTA^{4-}$, $DTPA^{5-}$, and $ODDA^{2-}$ complexes in the solid state (••) and in solution (—).

of distances (RDF) is taken into account by a superposition of two or three Gaussian distributions:

$$\chi(k) = \sum_{i=1}^{3} \frac{N_i}{kC_{1,i}^{\,2}} f(\pi, k) \exp\left(-\frac{2C_{1,i}}{\lambda(k)}\right) \exp(-2C_{2,i}k^2) \sin(2kC_{1,i} + \phi(\pi,k)) \quad (1)$$

N_i is the number of atoms in the *i*th scatterers' subshell; $C_{2,i} = \sigma^2$ is the subshell Debye−Waller (DW) factor, and $C_{1,i}$ is closely related to R_i, the interatomic distance averaged over the atoms composing the subshell.[30] $\lambda(k) = k/\Gamma$ is an adjustable function that models the low-*k* damping factors. As described previously,[8,28] the Γ parameter was allowed to vary during the fitting procedure for fine adjustment between theoretical calculations and experimental data. This parameter also allows for the compensation of the FT boundary effects and was found within the classical range of 0 to 0.1.

Phases and Amplitudes. The Eu^{2+} and Sr^{2+} XAFS data were analyzed using only phases $\phi(\pi, k)$ and amplitudes $f(\pi, k)$ calculated theoretically using the FEFF6 code.[13]

To mimic the possible environment of the complexed Eu^{2+} and Sr^{2+} ions in solution, theoretical backscattering phases and amplitudes were calculated up to 4 Å for clusters on the basis of the $[Sr(DOTA)(H_2O)][C(NH_2)_3]_2$, $[Sr(DTPA)(H_2O)][C(NH_2)_3]_3$, and Sr(ODDA) crystal structures for the Sr^{2+} complexes and on the basis of the $[Sr(DOTA)(H_2O)][C(NH_2)_3]_2$, $[Sr(DTPA)(H_2O)][C(NH_2)_3]_3$, $[Eu(DTPA)(H_2O)][C(NH_2)_3]_3$, and Sr(ODDA) crystal structures for the Eu^{2+} complexes.

In $[Sr(DOTA)(H_2O)][C(NH_2)_3]_2$ (Figure 5),[11] the Sr^{2+} ion is nine-coordinated in a capped-square antiprism geometry formed by four carboxylate oxygen atoms at a distance $M-O_{Ac}$ of 2.548 Å, four nitrogen atoms at a distance M−N of 2.731 Å, and one capping innersphere water molecule at a distance $M-O_w$ of 2.85 Å. These three characteristic distances lead to three different contributions in the EXAFS spectrum that can theoretically be fitted simultaneously.

In the quasi-isostructural $[Sr(DTPA)(H_2O)][C(NH_2)_3]_3$ (Figure 5) and $[Eu(DTPA)(H_2O)][C(NH_2)_3]_3$ complexes,[10] the metal ion is nine-coordinated in a distorted capped-square antiprism geometry formed by five carboxylate oxygen atoms at average distances $M-O_{Ac}$ of 2.565 (2.556−2.589) and 2.574 (2.562−2.600) Å, one capping innersphere water molecule at distances $M-O_w$ of 2.619 and 2.623 Å, and three nitrogen atoms at average distances M−N of 2.821 (2.769−2.910) and 2.808 (2.760−2.889) Å, respectively. Again, three characteristic sets of distances can be distinguished, leading to three different contributions in the EXAFS spectrum.

In the Sr(ODDA) solid compound (Figure 5),[10] the metal ion is nine-coordinated, also in a distorted capped-square antiprism geometry, formed by two carboxylate oxygen atoms at 2.527 and 2.593 Å, one extramolecular carboxylate oxygen atom at 2.544 Å coming from a neighboring complex, four ring-oxygen atoms at an average distance $M-O_{oxa}$ of 2.653 (2.626−2.702) Å, and two nitrogen atoms at an average distance M−N of 2.769 (2.762−2.776) Å. Because the two intramolecular, as well as the extramolecular, carboxylate oxygen atoms are located at very similar distances from the metal ion, their contributions cannot be distinguished. As a consequence, these atoms were fitted as a single contribution in the solid compound with an average distance of 2.555 Å. Finally, three characteristic sets of distances can once more be distinguished, corresponding to three different contributions in the EXAFS spectrum.

In each case, the first shell of scatterers can consequently be decomposed in three characteristic subshells, which can theoretically be fitted separately in the EXAFS spectrum. To allow for comparisons between the structural parameters fitted for the different compounds, the calculated backscattering phases and amplitudes were compared for similarity, within the precision limits, for similar atoms at similar distances in the different computed clusters.

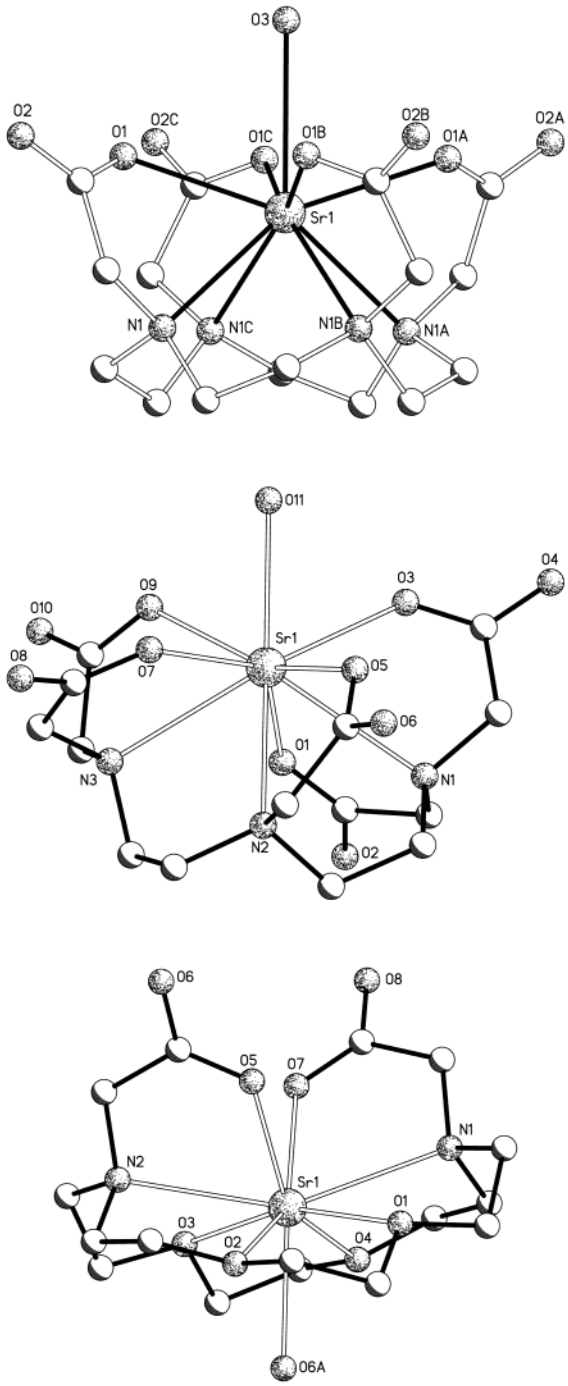

Figure 5. Ball-and-stick representation of the $[Sr(DOTA)(H_2O)][C(NH_2)_3]_2$, $[Sr(DTPA)(H_2O)][C(NH_2)_3]_3$, and Sr(ODDA) coordination polyhedra (from top to bottom).

Eu^{3+} Contamination. The low-energy part of the XAFS spectrum is called XANES and is very sensitive to both the valence and coordination polyhedron around the absorbing atom.[31] Figure 6 presents the Eu L_3-edge XANES spectra of the $[Eu(DOTA)(H_2O)]^{2-}$ complex in the solid state and in solution (see Figure S1 in Supporting Information for the $DTPA^{5-}$ and $ODDA^{2-}$ complexes). The spectra consist of a dominant white-line (WL) resonance (normalized amplitude 2.8−3.2 at 6974 eV) corresponding to the transition from the $2p_{3/2}$ level to the unoccupied 5d states, followed by important multiple-scattering contributions. In aqueous solution, the Eu^{2+} and Eu^{3+} valence states were easily distinguished because of the different threshold energies of their WLs ($\Delta E_0 \approx 8$ eV), and amounts of Eu^{3+} smaller than 1% could be detected by

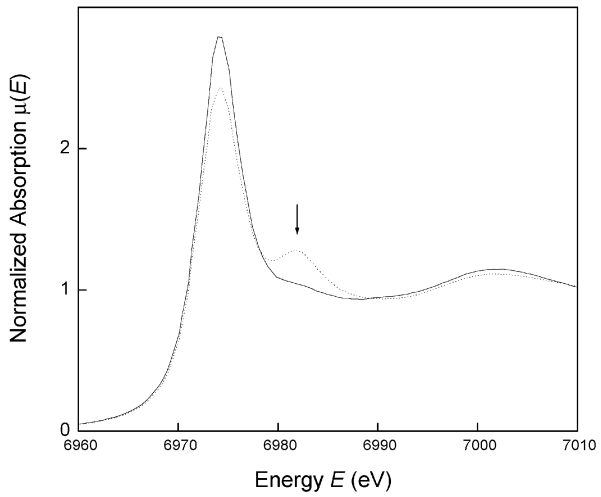

Figure 6. Eu L_3-edge XANES spectra of the $[Eu(DOTA)(H_2O)]^{2-}$ complex in the solid state (••) and in solution (—). The hump (see arrow) is due to Eu^{3+} contamination in the solid state.

XANES.[8] The Eu^{2+} DOTA,$^{4-}$ DTPA^{5-}, and ODDA^{2-} complexes with redox potentials of −1.18, −1.35, and −0.82 V ($E_{1/2}$ vs Ag/AgCl), respectively, are expected to be even more reactive toward oxidation than the aqua ion (−0.63 V).

Whereas the Eu^{2+} solution samples are practically Eu^{3+}-free, completely pure Eu^{2+} solid samples could not be obtained. From the XANES analysis (Figures 6 and S1), we estimated the Eu^{3+} contamination to be up to 10% in the case of the $[Eu(DOTA)(H_2O)][C(NH_2)_3]_2$ complex (6% for $[Eu(DTPA)(H_2O)][C(NH_2)_3]_3$ and 4% for Eu(ODDA)). The rough EXAFS spectrum of the $[Eu(DOTA)(H_2O)][C(NH_2)_3]_2$ complex was fitted to evaluate the uncertainties due to Eu^{3+} contamination on the fitted structural parameters. The distances obtained were quite reasonable, but the DW factors were far too large (0.019, 0.018, and 0.013 Å^2 for M−O_{Ac}, M−N, and M−O_w, respectively) essentially because of the error introduced by the Eu^{3+} atomiclike contribution μ_o[27,32] in the normalization process. Moreover, for Eu^{2+} poly(amino carboxylate), as for other Eu^{2+} compounds,[8] the experimental XAFS spectra $\chi(E)$ of the Eu^{2+} and Eu^{3+} complexes show destructive interference due to their different E_0 energies. Since the Eu^{3+} EXAFS spectrum is about twice as high as that of Eu^{2+}, even small amounts of Eu^{3+} in solution can interfere with the analysis of Eu^{2+} XAFS spectra and could lead to a misinterpretation of the data.

To correct the XAFS spectra from the Eu^{3+} contamination, experimental XAFS spectra of the Eu^{3+} DOTA^{4-}, DTPA^{5-}, and ODDA^{2-} solid complexes were measured under identical conditions to those for the Eu^{2+} and Sr^{2+} solid compounds. The spectra were corrected for the background contribution μ_b[27,32] before the corresponding Eu^{3+} complex contributions were subtracted from the contaminated Eu^{2+} spectra. The corrected spectra were then analyzed as described in the Data Analysis section.

Multielectron Transition Effect. As in the case of the aqua ion[8] and in the case of the free Eu^{2+} ion in nonaqueous solvents,[28] a sharp contribution due to a 2p4d double-electron transition (indicated by arrows in Figure 1) is observed around 6.2 Å^{-1} in the EXAFS spectrum of the Eu^{2+} complexes with DOTA,$^{4-}$ DTPA^{5-}, and ODDA^{2-} ligands. Such an anomalous contribution is not distinctively visible in the EXAFS spectrum of the supposedly isostructural Sr^{2+} complexes (see arrows in Figure 2) whereas a sharp contribution due to the simultaneous excitation of 1s3d electrons was clearly observed around 6.4 Å^{-1} for Sr^{2+} in aqueous and nonaqueous solutions. The presence

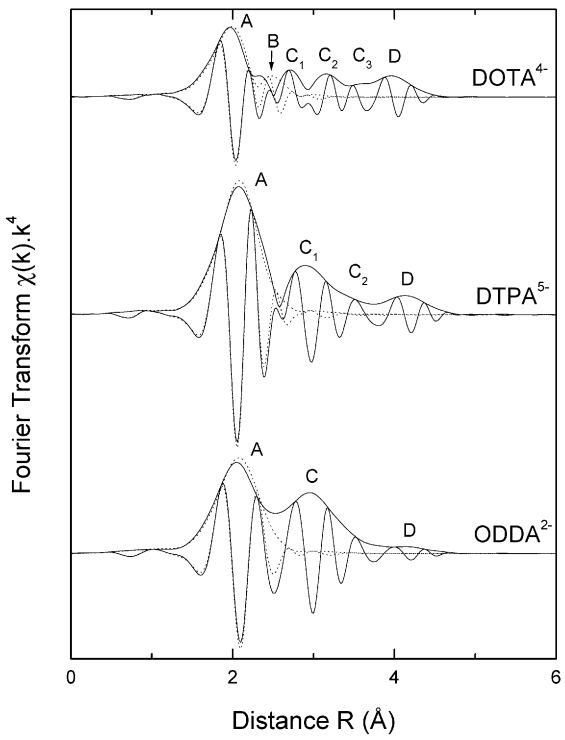

Figure 7. Fourier transforms (modulus and imaginary parts) of the theoretical XAFS $\chi(k)k^4$ spectra of the Sr^{2+} DOTA^{4-}, DTPA^{5-}, and ODDA^{2-} complexes (—) with their respective first shell of scatterers' contributions (••) based on crystallographic coordinates.

of a structural peak in the EXAFS spectrum of the Sr^{2+} poly(amino carboxylates) could, for instance, mask such a low-intensity contribution.

Finally, even if these multielectron transition (MET) effects slightly distort the base of the first peak at small distances,[8,28] the use of the 2001 EDA software package[27] combined with the use of the k^3 and k^4 compensation factors prevents any additional MET removal after the Fourier filtering process.

Results

In the EXAFS study of the Eu^{2+} and Sr^{2+} aqua ions in aqueous solution,[8] only one type of scatterer was present. As a consequence, the single scattering from the first shell of scatterers was analyzed quantitatively without difficulty. In the dimethyl sulfoxide (DMSO) solution, the sulfur atoms of the coordinated solvent molecules formed a second shell of scatterers, leading to additional single-scattering (SS) and multiple-scattering (MS) contributions.[28] In the poly(amino carboxylate) complexes, different types of atoms constitute the first shell of scatterers. Additionally, the rigidity of the complex cages leads to significant SS and MS contributions of the outer shells of scatterers, further complicating the experimental XAFS spectrum.[12,26]

Theoretical calculations based on the crystallographic structures of the $[Sr(DOTA)(H_2O)][C(NH_2)_3]_2$, $[Sr(DTPA)(H_2O)][C(NH_2)_3]_3$, and Sr(ODDA) complexes using the FEFF6 code[13] were performed to understand the Eu^{2+} and Sr^{2+} experimental XAFS spectra. Figure 7 shows that for both DTPA^{5-} and ODDA^{2-} complexes the first shell of scatterers is well defined and well separated from the outer contributions. The calculated spectrum is more complicated for the DOTA^{4-} complex; the first sphere contribution (Figure 7) does not consist of only one dominant peak but of one major peak A (half as intense as that for the DTPA^{5-} complex) followed by a smaller peak B due to

destructive interference between the $M-O_{Ac}$, $M-N$, and $M-O_w$ contributions. The calculations also show that peak B cannot be singled out precisely from the experimental spectrum, leading to uncertainties in the determination of the $M-O_w$ distance.

For the three DOTA,$^{4-}$ DTPA^{5-}, and ODDA^{2-} complexes, peak A corresponds to the first peak of scatterers, as already described in the Experimental Section. The following peaks labeled C correspond to the carbon atoms of the carboxylate function of the acetate arms and of the ethylenic groups, but the peaks cannot be assigned individually (with and without taking into account MS contributions). Finally, peak D corresponds to the uncoordinated carboxylate oxygen atoms. Calculations also show that a number of low-amplitude MS contributions that could give significant contributions to the C and D peaks occur in the poly(amino carboxylate) EXAFS spectra starting around 3.5 Å.

The general patterns predicted by the theoretical calculations are effectively observed on the experimental FT spectra, with a somewhat lower resolution on the Eu^{2+} L_3-edges (Figure 3) than on the Sr^{2+} K-edges (Figure 4). Deviations from the calculated spectrum do occur, as the DW factors characterizing the outer spheres of scatterers and the MS contributions could not be predicted accurately and are subjected to thermal vibrations. In all cases, the FT imaginary part shows more specifically that the structure observed in the solid state is globally retained in solution. That peak D is so intense in the experimental spectrum is quite remarkable, as it corresponds to atoms located quite far from the metal ion. In the solid-state structures of $[Sr(DTPA)(H_2O)][C(NH_2)_3]_3$, $[Eu(DTPA)(H_2O)][C(NH_2)_3]_3$, and Sr(ODDA), noncoordinated crystallized water molecules are located at a similar distance (but were omitted from the theoretical calculations and Figure 7). In the structures of $[Sr(DOTA)(H_2O)][C(NH_2)_3]_2$, $[Sr(DTPA)(H_2O)][C(NH_2)_3]_3$, and $[Eu(DTPA)(H_2O)][C(NH_2)_3]_3$, nitrogen atoms from the guanidinium counterions (again omitted from the theoretical calculations and Figure 7) are also found at the same distance. This explains the high intensity of the D peak in the solid state. The experimental spectra moreover suggest that these spaces are accessible in solution to second-sphere water molecules.

As discussed, the contributions of the outer shells of scatterers are numerous and cannot be easily gathered into coherent and distinct subgroups. With two fitting parameters per contribution (i.e., distance and DW factor), the maximum number of fitting parameters would be easily reached, leading to strongly enhanced correlation among parameters. Thus, the first shell of scatterers was singled out and fitted separately.

The number of fitting parameters is limited by the number of independent data points $N_{ind} \cong 2\Delta k\Delta R/\pi + 2$, where Δk and ΔR are the k and the R ranges used.[33] For the study of the first shell of scatterers of the poly(amino carboxylates), three-contribution models (as described in the Experimental Section) were considered. Each contribution was characterized by two fitting parameters (i.e., distance and DW factor (N_{ind}, Δk, and ΔR values are detailed in Table S1)). In addition, two contribution models were considered to check the physical significance of the proposed models.

In the solid state, the coordinated water molecule of the $[Sr(DOTA)(H_2O)][C(NH_2)_3]_2$ complex seems to be loosely bound to the metal ion. The $[M^{II}(DOTA)(H_2O)]^{2-}$ complexes ($M^{II} = Eu^{2+}$, Sr^{2+}) in solution with $4 \times O_{Ac}$ and $4 \times N$ subshell models were analyzed for the presence of an innersphere water molecule. Similarly to the $[Gd(DOTA)(H_2O)]^-$ and $[Gd(DTPA)(H_2O)]^{2-}$ complexes,[12] a two-subshells model including one innershell water molecule was sufficient to fit the EXAFS spectra of the $[M^{II}(DOTA)(H_2O)]^{2-}$ complexes ($M^{II} = Eu^{2+}$, Sr^{2+}). For the DOTA^{4-} complexes, however, the use of $5 \times O_{Ac}$ and $4 \times N$ subshell models led to unrealistic DW factor and distance values, confirming that the innersphere water molecule has to be fitted separately. The presence of the water molecule was then tested at different distances from the metal ion, and the only feasible results were obtained with $M-O_w > M-N$. Table 1 shows that the fitted $M-O_w$ distances for the DOTA^{4-} complexes are slightly larger than the crystallographic distances. The fitted distance that is excessively large is due to partial overlap between the first-shell B peak and the outer shells' contribution (Figure 7), which prevents the first shell of scatterers from being precisely singled out. For the same reasons, the corresponding DW factor values are smaller than their true values, which cannot be measured from experimental data. Nevertheless, fitting gave very close distances and DW factor values for both Eu^{2+} and Sr^{2+} complexes in both the solid state and in solution, indicating the consistency of the analyses. This consistency allows the $M-O_w$ distance in the $[M^{II}(DOTA)(H_2O)]^{2-}$ complexes ($M^{II} = Eu^{2+}$, Sr^{2+}) to be estimated as 2.85(5) Å. The reliability of the $M-O_w$ distance in the $[M^{II}(DTPA)(H_2O)]^{3-}$ complexes was similarly checked. Estimated from the EXAFS fitting results as 2.62(5) Å, the $M-O_w$ distance is slightly increased in solution, but the overall structure remains the same, albeit slightly swelled.

The ^{17}O NMR chemical shift measurements on the Eu(ODDA) complex[10] show that the extramolecular carboxylate oxygen atom coordinating the metal ion in the solid state is replaced by a water molecule in aqueous solution. The presence of this water molecule was verified using XAFS data in solution with $2 \times O_{Ac}$, $4 \times O_{oxa}$, and $2 \times N$ subshell models. The distances and DW factors of the $(2 \times O_{Ac} + 1 \times O_{ax})$ subshell are very similar in the solid state and in solution, indicating that even if the water molecule cannot be located precisely it clearly stands inside the first subshell. Consequently, the $M-O_{ax}$ distance is virtually unchanged in the solid state and in solution. A swelling tendency was observed within the DTPA^{5-} complexes, whereas the ODDA^{2-} complexes seem to undergo more subtle changes: In the solid state, one carboxylate group bridges two Sr^{2+} ions (Figure 5), leading to a slightly longer $M-O_{Ac}$ distance than observed for the other carboxylate arm.[10] In solution, the two acetate arms are equivalent, leading to a slight shortening of the $M-O_{Ac}$ average distance and consequently to a subtle reorganization of the overall structure. Therefore, in the $[M^{II}(ODDA)(H_2O)]$ complexes, the $M-O_w$ distance in aqueous solution can be estimated from the EXAFS fitting results to be 2.54(5) Å.

Table 1 summarizes the characteristic distances and DW factors obtained for the metal ion first shell of scatterers in the different complexes. In multishell systems, systematic errors are predominant and were accounted for in the table, together with statistical errors. Statistical errors (Table S1) were estimated by extensive fitting of the experimental first-shell XAFS spectra, and outside the fitting intervals indicated, the fitting errors were at least doubled. The distances obtained for the first shell of scatterers (Table 1) in the Eu^{2+} and Sr^{2+} complexes in the solid state and in solution are in good agreement with the distances observed by XRD with respect to the experimental errors. Therefore, the overall structure of the different complexes is globally conserved from the solid state to the solution and from the Sr^{2+} ion to the Eu^{2+} ion.

The XAFS experimental spectra after the first-shell filtering of the $[M^{II}(DOTA)(H_2O)]^{2-}$, $[M^{II}(DTPA)(H_2O)]^{3-}$, and $M^{II}(ODDA)$ complexes ($M^{II} = Eu^{2+}$, Sr^{2+}) in the solid state

TABLE 1: First Shell of Scatterers Structural Data Obtained from XAFS Analysis with Theoretical Phase and Amplitude at Room Temperature and Comparison with X-ray Diffraction Data[a]

DOTA^{4-} Ligand

	4 × M−O_{Ac}		4 × M−N		1 × M−O_w	
sample	R(Å)	C_2(Å^2)	R(Å)	C_2(Å^2)	R(Å)	C_2(Å^2)
[Eu(DOTA)(H_2O)][$C(NH_2)_3$]$_2$	2.57(2)	0.011(1)	2.78(2)	0.008(1)	2.94(2)	0.004(1)
[Eu(DOTA)(H_2O)]$^{2-}$ 0.2 M	2.59(2)	0.011(1)	2.79(2)	0.009(2)	2.94(3)	0.006(2)
[Sr(DOTA)(H_2O)][$C(NH_2)_3$]$_2$ [b]	2.548		2.731		2.85	
[Sr(DOTA)(H_2O)][$C(NH_2)_3$]$_2$	2.56(2)	0.009(1)	2.78(2)	0.008(1)	2.94(3)	0.004(1)
[Sr(DOTA)(H_2O)]$^{2-}$ 0.2 M	2.58(2)	0.009(1)	2.77(2)	0.007(1)	2.92(3)	0.004(1)

DTPA^{5-} Ligand

	5 × M−O_{Ac}		1 × M−O_w		3 × M−N	
sample	R(Å)	C_2(Å^2)	R(Å)	C_2(Å^2)	R(Å)	C_2(Å^2)
[Eu(DTPA)(H_2O)][$C(NH_2)_3$]$_3$ [b]	2.574		2.623		2.808	
[Eu(DTPA)(H_2O)][$C(NH_2)_3$]$_3$	2.56(2)	0.011(2)	2.58(3)	0.009(3)	2.77(2)	0.008(3)
[Eu(DTPA)(H_2O)]$^{3-}$ 0.1 M	2.58(2)	0.012(2)	2.62(3)	0.008(2)	2.80(2)	0.010(2)
[Sr(DTPA)(H_2O)][$C(NH_2)_3$]$_3$ [b]	2.565		2.619		2.821	
[Sr(DTPA)(H_2O)][$C(NH_2)_3$]$_3$	2.55(2)	0.011(1)	2.58(2)	0.005(1)	2.76(2)	0.014(1)
[Sr(DTPA)(H_2O)]$^{3-}$ 0.1 M	2.56(2)	0.012(1)	2.64(4)	0.009(2)	2.79(3)	0.013(2)

ODDA^{2-} Ligand

	2 × M−O_{Ac} + 1 × M−O_{ax}[c]		4 × M−O_{oxa}		2 × M−N	
sample	R(Å)	C_2(Å^2)	R(Å)	C_2(Å^2)	R(Å)	C_2(Å^2)
[Eu(ODDA)]	2.55(2)	0.010(1)	2.70(2)	0.010(1)	2.83(2)	0.009(1)
[Eu(ODDA)(H_2O)] 0.1 M	2.54(2)	0.007(1)	2.66(2)	0.010(1)	2.90(3)	0.009(1)
[Sr(ODDA)][b]	2.555		2.653		2.769	
[Sr(ODDA)]	2.52(2)	0.010(1)	2.62(2)	0.006(1)	2.80(2)	0.007(1)
[Sr(ODDA)(H_2O)] 0.1 M	2.53(2)	0.012(1)	2.63(2)	0.010(1)	2.84(3)	0.012(1)

[a] For each subshell of scatterers at an average distance R from the metal, $C_2 = \sigma^2$ is the DW factor. Estimated errors (both statistical and systematic) are presented within parentheses. [b] Average crystallographic data (see text). [c] O_{ax} comes from a carboxylate group in the solid state and from a coordinated water molecule in solution.

and in aqueous solution are presented in Figure S1 together with the fitted spectra with theoretical phases and amplitudes. The low residual intensities (dotted lines) demonstrate the quality of these fits.

Discussion

Structural Comparison between Eu^{2+} and Sr^{2+} Complexes. Our EXAFS study of the Eu^{2+} and Sr^{2+} solvation in aqueous and nonaqueous solvents[28] showed that the Eu^{2+} and Sr^{2+} ionic radii should be considered to be equivalent for the same coordination number. Furthermore, Eu^{2+} seems to be a slightly softer ion than Sr^{2+}, leading to shorter M−N and longer M−O bonds and to smaller coordination numbers in O-coordinating solvents. For instance, in aqueous solution, the $[Eu(H_2O)_7]^{2+}$ and $[Sr(H_2O)_8]^{2+}$ ions feature a 1-unit solvation number difference as well as a 0.016 Å M−O bond length difference. These differences are directly visible (differences in amplitude and in periodicity) when comparing the corresponding crude experimental EXAFS spectra (Figure 8a).

Polydentate ligands are usually more structuring than monodentate ligands and frequently dictate the coordination geometry around the metal center. The poly(amino carboxylate) ligands can therefore force the Eu^{2+} and Sr^{2+} ions into very close coordination polyhedrons that are hardly distinguishable in their crude experimental EXAFS spectra (Figure 8b). In the $[M^{II}(DOTA)(H_2O)]^{2-}$, $[M^{II}(DTPA)(H_2O)]^{3-}$, and $[M^{II}(ODDA)(H_2O)]$ (M^{II} = Eu^{2+} or Sr^{2+}) complexes, the first shell of scatterers can be split into three characteristic subshells that can be fitted separately in the EXAFS spectrum (see Experimental Section). Because of the large number of contributions needed for the analysis of the first shell of scatterers of the poly(amino carboxylate) complexes (Table 1), the fitting errors are 1 order of magnitude higher than in the case of the solvates. Hence, within the XAFS fitting errors, the distances obtained for the first shell of scatterers of both Eu^{2+} and Sr^{2+} ions (Table 1) in the DOTA,$^{4-}$ DTPA^{5-}, and ODDA^{2-} complexes are very

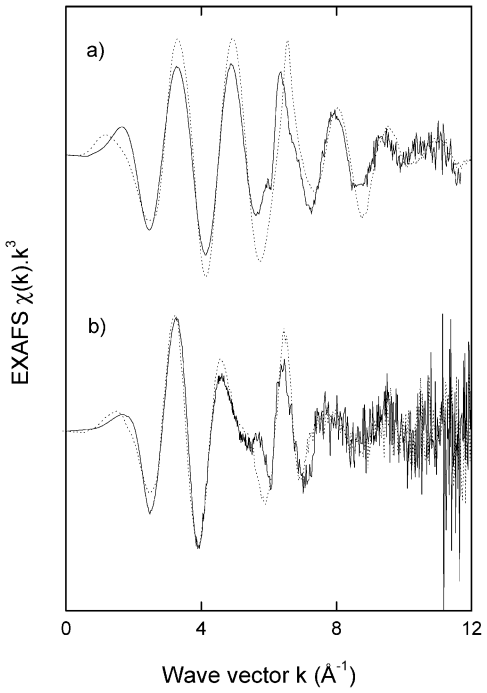

Figure 8. Correction-free experimental $\chi(k)k^3$ XAFS spectra of (a) 0.15 M $[Eu(H_2O)_7]^{2+}$ (—) and 0.14 M $[Sr(H_2O)_8]^{2+}$ (••) ions in aqueous solution and (b) 0.1 M [Eu(ODDA)(H_2O)] (—) and [Sr(ODDA)(H_2O)] (••) complexes in aqueous solution. The phases of the Eu^{2+} spectra were inverted for clarity.

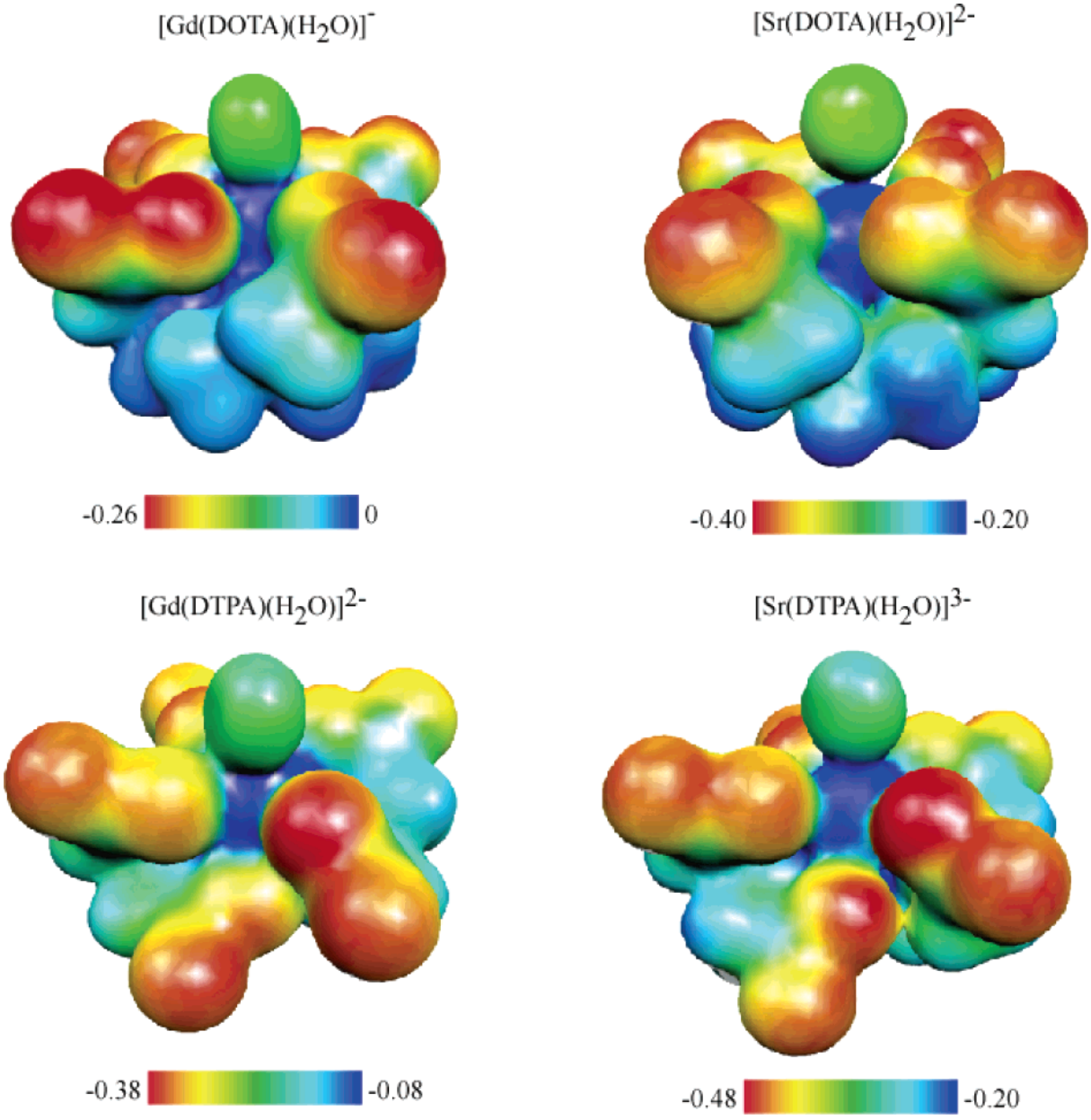

Figure 9. Electrostatic potential (au) plotted on the electronic density maps of the Sr^{2+} and Gd^{3+} $DOTA^{4-}$ and $DTPA^{5-}$ complexes. Only the oxygen atom of the water molecule has been represented.

SCHEME 2: Schematic Structure of the Two Diastereoisomers of the $DOTA^{4-}$ Complexes[a]

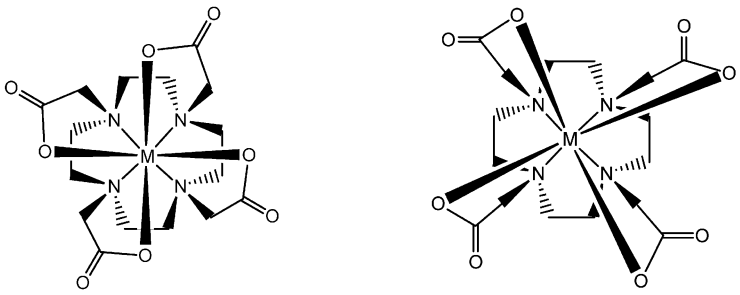

Square Antiprism (SA or M) Isomer **Twisted Square Antiprism (TSA or m) Isomer**

[a] Coordinated water molecule has been omitted for clarity.

similar for the same subshell in both the solid state and in solution and are in good agreement with the distances observed by X-ray diffraction (XRD). This latter method gives access to more precise distances for the solid-state complexes and indicates that the Eu−O bond lengths are 0.015 Å longer in the XRD structures of isomorphous acetates[34,35] than in their Sr^{2+} homologues. In the $[Eu(DTPA)(H_2O)][C(NH_2)_3]_3$ and $[Sr(DTPA)(H_2O)][C(NH_2)_3]_3$ XRD structures,[10] the M−N bond lengths are shorter on average by 0.013 Å, and M−O bond lengths are 0.011 Å longer for the Eu^{2+} than for the Sr^{2+} ion.

SCHEME 3: Scaled Schematic Description of the Metal Position in the Sr^{2+} and Gd^{3+} $DOTA^{4-}$ and $DTPA^{5-}$ Complexes[a]

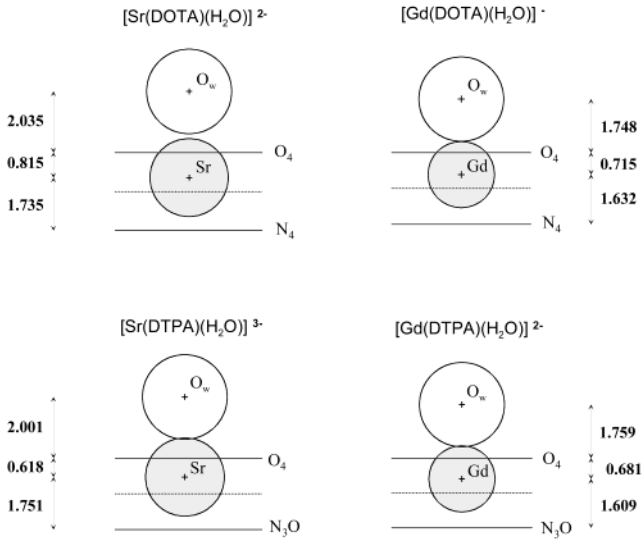

[a] Basal and apical planes are represented by a solid line, and the midplane is represented by a dotted line. The radii used to represent the Sr^{2+} and Gd^{3+} metal ions and the coordinated water oxygen atom correspond to the ionic radii determined by Shannon[2] for nine coordination (1.31, 1.107, and 1.40 Å, respectively). Distances between the basal plane, the metal ion, the apical plane, and the coordinated water oxygen atom are given in angstroms.

Within the XAFS fitting errors, the distances obtained for the first shell of scatterers (Table 1) of the $DOTA^{4-}$ and $DTPA^{5-}$ complexes in both the solid state and in solution are very similar for both the Eu^{2+} and Sr^{2+} ions. In the $ODDA^{2-}$ complexes, the overall complex structure is rearranged slightly from the solid state to the solution (see Results section), with the bridging carboyxylate group being replaced by a coordinating water molecule. In summary, the overall structure of these poly(amino carboxylate) complexes is globally conserved from the solid state to solution. Thus, the structure of the Eu^{2+} and Sr^{2+} poly(amino carboxylate) complexes in solution can be discussed on the basis of the XRD structure of the isostructural solid-state Sr^{2+} complexes.

Solution and Solid-State Structures of the M^{II} (M^{II} = Eu^{2+}, Sr^{2+}) and Gd^{3+} Poly(amino carboxylates). In the nine-coordinated $DOTA^{4-}$ complexes, the metal ion coordination polyhedron consists of capped-square antiprisms. The two square planes are formed by the four ring nitrogen atoms (N_4 basal plane) and the four coordinated carboxylate oxygen atoms (O_4 apical plane). The water molecule caps the apical plane. In the $DTPA^{5-}$ complexes, the metal ion is coordinated in distorted capped-square antiprisms. The three nitrogen atoms and a terminal carboxylate oxygen atom form the basal plane (N_3O), and the four other coordinated carboxylate oxygen atoms form the apical plane (O_4), where the water molecule is coordinated. In all of the Gd^{3+} $DOTA^{4-}$ and $DTPA^{5-}$ derivatives, for which XRD structures are known,[20,21,36-38] both Gd^{3+} ion positions inside the ligand cavity (with respect to the basal and apical planes) and the $Gd-O_w$ distances (from 2.43 to 2.46 Å) are very close.

In the $[MII(DOTA)(H_2O)]^{2-}$ (M^{II} = Eu^{2+}, Sr^{2+}) complexes studied here, the $DOTA^{4-}$ ligand is structurally reorganized around the metal ion to accommodate these larger ions (Figure 9). All of the solid-state X-ray structures of Gd^{3+} $DOTA^{4-}$ derivatives exhibit a square antiprismatic (SA) conformation (Scheme 2) characterized by a twist angle between the O_4 and N_4 planes close to 39° (39.3° in the $[Gd(DOTA)(H_2O)]^-$ complex). In the $[M^{II}(DOTA)(H_2O)]^{2-}$ complexes, the twist angle is −24.8°, characteristic of a twisted-square antiprismatic (TSA) conformation (Scheme 2).[20,39-41] The change of conformation of the carboxylate arms leads to an increase in the cavity size of 0.2 Å (an increase in the distance between the basal and apical planes; see Scheme 3). Consequently, despite their larger ionic radii, the Eu^{2+} and Sr^{2+} ions are located slightly deeper inside the $DOTA^{4-}$ cavity than the Gd^{3+} ion (the position of

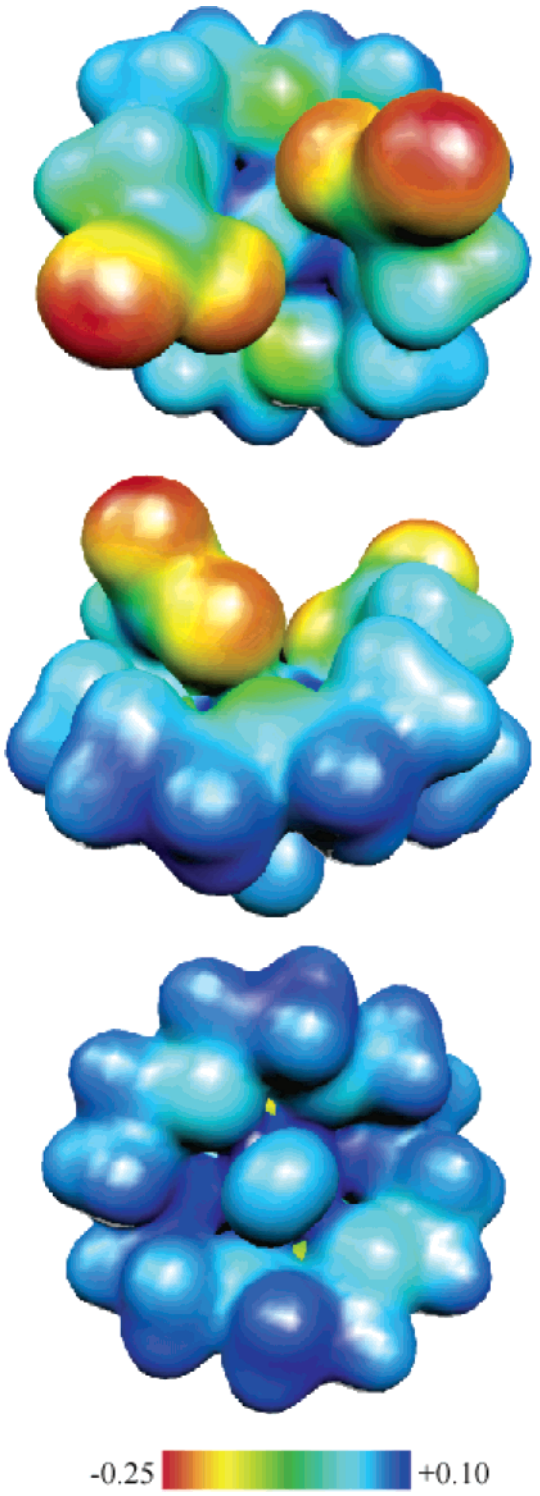

Figure 10. Electrostatic potential (au) plotted on the electronic density map of the [Sr(ODDA)(H_2O)] complex (from top to bottom: carboxylate coordinating site, side view, and water-coordinating site). Only the oxygen atom of the water molecule has been represented.

TABLE 2: Selected Constants Characterizing the Solution Structure and Water Exchange of the Eu^{2+} and Gd^{3+} Poly(amino carboxylate) Complexes[a]

complex	$[Eu(H_2O)_7]^{2+}$	$[Eu(DOTA)(H_2O)]^{2-}$	$[Eu(DTPA)(H_2O)]^{3-}$	$[Eu(ODDA)(H_2O)]$	$[Gd(H_2O)_8]^{3+}$	$[Gd(DOTA)(H_2O)]^{-}$	$[Gd(DTPA)(H_2O)]^{2-}$
$M-O_w$ (Å)	2.584(5) [b]	2.85(5)[c,d]	2.62(5)[d]	2.54(5)[d]	2.41(1) [g]	2.46(5)[g]	2.47(5)[g]
$\Delta V^{\ddagger}$ ($cm^3\ mol^{-1}$)	−11.3 [b]	+0.1[e]	+4.5[f]	−3.9[f]	−3.3[h]	+10.5[i]	+12.5[i]
mechanism	A[b]	I[e]	I_d[f]	I_a[f]	A[h]	D[i]	D[i]
K_{ex}^{298} (s^{-1})	5×10^9 [b]	2.46×10^9 [e]	1.3×10^9 [f]	0.43×10^9 [f]	0.8×10^9 [h]	4.1×10^6 [i]	3.3×10^6 [i]

[a] $M-O_w$ distances are obtained from XAFS analysis; $\Delta V^{\ddagger}$ and K_{ex}^{298} are respectively the activation volume and the rate constant at 25 °C of the water-exchange reaction. [b] Reference 8. [c] X-ray value (see text). [d] This study. [e] Reference 11. [f] Reference 10. [g] Reference 12. [h] Reference 48. [i] Reference 46.

the metal ion inside the cavity is characterized by the ratio between the $M-O_4$ and O_4-N_4 distances to account for the different cavity sizes).

The conformational reorganization occurring from the Gd^{3+} to the $[M^{II}(DTPA)(H_2O)]^{3-}$ complexes is much smaller (Figure 9). The $DTPA^{5-}$ ligand has no opportunity to reorganize itself to generate a larger cavity, and the larger Eu^{2+} and Sr^{2+} ions are, on the contrary, shifted from the center of the cavity toward the O_4 plane (Scheme 3). Thus, the Eu^{2+} and Sr^{2+} ions lie about 0.2 Å closer to the O_4 plane in the $DTPA^{5-}$ complexes than in the $DOTA^{4-}$ complexes.

The $M^{II}-O_w$ distance is more than 0.2 Å longer in the $[M^{II}(DOTA)(H_2O)]^{2-}$ ($M^{II} = Eu^{2+}$ or Sr^{2+}) complexes than in the $[M^{II}(DTPA)(H_2O)]^{3-}$ complexes whereas the $Gd-O_w$ distance is approximately the same in the $[Gd(DOTA)(H_2O)]^{-}$ and $[Gd(DTPA)(H_2O)]^{2-}$ complexes.[20,21] In these latter complexes, the position of the water molecule results from the attraction of the metal cation and from the repulsion of the coordinating carboxylates that define the capping site. In both the $[M^{II}(DOTA)(H_2O)]^{2-}$ and $[M^{II}(DTPA)(H_2O)]^{3-}$ ($M^{II} = Eu^{2+}$ or Sr^{2+}) complexes, the water molecule is located at a distance of $R = 2.0$ Å from the O_4 apical plane (Scheme 3). In the $[Gd(DOTA)(H_2O)]^{-}$ and $[Gd(DTPA)(H_2O)]^{2-}$ complexes,[20,21] this distance R is shortened to 1.75−1.76 Å and is practically identical for the two complexes. Among the Gd^{3+} $DOTA^{4-}$ and $DTPA^{5-}$ derivatives, R ranges from 1.71 to 1.76 Å.[36−38] Therefore, for the same metal ion, R appears to be only slightly dependent on the charge and ligand substituents. The repulsive effect of the carboxylate functions is responsible for this R distance, but the 0.25 Å shortening observed from the M^{2+} to the Gd^{3+} ions can be explained only by the higher charge density on the trivalent Gd^{3+} ion (higher charge and smaller ionic radius). Thus, the difference in the $M^{II}-O_w$ distance between the $[M^{II}(DOTA)(H_2O)]^{2-}$ and $[M^{II}(DTPA)(H_2O)]^{3-}$ ($M^{II} = Eu^{2+}$ or Sr^{2+}) complexes is completely explained by the difference in the $M-O_4$ distance resulting from the various positions of the metal ion in the ligand cavity. The position of the Gd^{3+} ion inside the complex cavities is very similar in the $DOTA^{4-}$ and $DTPA^{5-}$ derivatives; therefore, it could be predicted that the 0.2 Å $M^{II}-O_w$ difference also occurs between the M^{II} $DOTA^{4-}$ and $DTPA^{5-}$ derivatives.

In the solid-state complex Sr(ODDA),[10] the metal ion is coordinated by an extramolecular carboxylate oxygen atom (Figure 5). The ^{17}O NMR chemical shifts measured on Eu(ODDA) solutions[10] clearly indicate the presence of an innersphere water molecule replacing the extramolecular carboxylate in solution, as confirmed by our XAFS measurements. The innersphere water molecule and the intramolecular carboxylates coordinate the metal ion from opposite sides of the macrocyclic plane (Figure 5). The water molecule coordinating site is far less crowded and less electrostatically constrained in the $ODDA^{2-}$ complexes than in the $DOTA^{4-}$ or $DTPA^{5-}$ complexes (Figures 9 and 10). It could be speculated that a second water molecule coordinates the metal ion in solution, but both the XAFS and the ^{17}O NMR chemical shift measurements[10] show that the Eu(ODDA) complex occurs in aqueous solution as a monohydrated species.

The unique design of the $ODDA^{2-}$ complex makes it hardly comparable with the $DOTA^{4-}$ and $DTPA^{5-}$ complexes, except for the $M-O_w$ distance. Our XAFS study of the Eu^{2+} and Sr^{2+} aqua ions in aqueous solution[8] led to $M^{II}-O_w$ distances of 2.584(5) and 2.600(3) Å. In the $DTPA^{5-}$ complex, this distance is slightly increased by about 0.04 Å. In the $DOTA^{4-}$ complex, this distance increases to 2.85 Å for structural reasons. The $M^{II}-O_w$ distance in the $[M^{II}(ODDA)(H_2O)]$ complexes was estimated in aqueous solution to be low, 2.54(5) Å. In the $ODDA^{2-}$ complexes, the water-coordinating site is very open, and the coordinated water molecule does not suffer any carboxylate electrostatic repulsion. The $M^{II}-O_w$ distances in the $[M^{II}(ODDA)(H_2O)]$ complexes are therefore very close to the ones observed for the $[Eu(H_2O)_7]^{2+}$ and $[Sr(H_2O)_8]^{2+}$ ions (Table 2).

Structural Consequences for the Water Exchange Reaction on Eu^{2+} and Gd^{3+} Poly(amino carboxylates). The $DOTA^{4-}$ derivative complexes of the trivalent lanthanide ions occur in aqueous solution as an equilibrium between SA and TSA isomers (also called M and m isomers), the m/M ratio being very low for the smaller ions and very close to 1 for the La^{3+} and Ce^{3+} ions.[42] It has been shown that the exchange of the coordinated water molecule is much faster in TSA than in SA isomers.[43,44] The water exchange reaction (both the rate and mechanism) is then greatly influenced by the structure adopted by the complex in solution. The water exchange rate constant is strongly dependent on the $M-O_w$ bond properties and can therefore be related to the $M-O_w$ distance. Table 2 presents selected constants characterizing the structure and dynamics of the Eu^{2+} and Gd^{3+} aqua ions and poly(amino carboxylate) complexes in aqueous solution.

In the $[Gd(DOTA)(H_2O)]^{-}$ and $[Gd(DTPA)(H_2O)]^{2-}$ complexes, the entering water molecule can be coordinated only to the site of the leaving water molecule (Figure 9) and cannot participate in the bond-breaking process, leading to limiting dissociative (D) reaction mechanisms and a relatively slow exchange rate compared with that of the $[Gd(H_2O)_8]^{3+}$ ion, which features a limiting associative (A) mechanism (Table 2).[45,46] In these two complexes, all of the characteristic distances of the Gd^{3+} coordination polyhedron including the $Gd-O_w$ distance are approximately the same (Table 2). The water exchange rates are also similar for the two complexes, with a slight 20% increase from the $[Gd(DTPA)(H_2O)]^{2-}$ to the $[Gd(DOTA)(H_2O)]^{-}$ complex.

The mechanism of the $[Gd(DTPA)(H_2O)]^{2-}$ complex is limiting dissociative (D) whereas the $[Eu(DTPA)(H_2O)]^{3-}$ complex features a dissociative interchange (I_d) mechanism,[9] where the approach of another water molecule helps the departure of the coordinated water molecule. This difference in mechanism could be explained by the substantially longer $M-O_w$ distances as well as the lower charge density on the

metal ion (lower charge and larger ionic radius), both inducing weaker interactions between the metal center and the coordinated water molecule and a greater ability to break the $M-O_w$ bond. In addition, this weaker interaction is explicitly shown by the difference in electronic density between the metal ion and the water oxygen atom.

In the $[Eu(DOTA)(H_2O)]^{2-}$ complex, the $Eu-O_w$ distance is even longer (Table 2). The water molecule is very loosely coordinated and markedly less bound to the metal center than in the $[Eu(DTPA)(H_2O)]^{3-}$ complex. Once again, the weaker interaction is clearly seen in Figure 9 by the differences in the electronic density between the metal ion and the water oxygen atom. An entering water molecule can participate in the bond-breaking process, leading to an interchange (I) mechanism.[11] This shift in mechanism is associated with a large 0.2 Å increase in $M-O_w$ distance and leads, for the Eu^{2+} ion, to an increase in the water exchange rate from the $[Eu(DTPA)(H_2O)]^{3-}$ to the $[Eu(DOTA)(H_2O)]^{2-}$ complex (Table 2) by a factor of 2.

The $[Eu(ODDA)(H_2O)]$ complex features an associative interchange (I_a) water exchange mechanism.[10] In the transition state, the water-coordinating site accommodates a second water molecule, leading to the concerted departure of the previously coordinated molecule. A limiting associative (A) mechanism involving the coordination of a second innersphere water molecule prior to the departure of the leaving molecule is barely conceivable, the potential binding site not being large enough to accommodate two water molecules simultaneously (Figure 10 bottom). A dissociative activation mode is highly disfavored because of the very short $M-O_w$ distance (Table 2); therefore, an I_a mechanism is privileged. Note that a progressive change in the water exchange mechanism from D to I_d to I with increasing ionic radius has already been observed in the case of the $[Ln(DTPA-BMA)(H_2O)]$ complexes along the lanthanide series.[47]

Conclusions

This XAFS study establishes the similarity of the Eu^{2+} and Sr^{2+} poly(amino carboxylates) structures in the solid state and in solution. In addition, the overall solid-state structure is conserved in solution. We showed that the $DOTA^{4-}$ ligand adopts a twisted-square antiprismatic conformation in aqueous solution to accommodate the large Eu^{2+} and Sr^{2+} ions, leading to a metal ion-to-coordinated water distance in the $[M^{II}(DOTA)(H_2O)]^{2-}$ complexes that is 0.2 Å longer than in the $[M^{II}(DTPA)(H_2O)]^{3-}$ ($M^{II} = Eu^{2+}$, Sr^{2+}) complexes. The study of the solid-state structures of the Gd^{3+} $DOTA^{4-}$ and $DTPA^{5-}$ derivatives shows that this 0.2 Å difference should occur in the M^{II} $DOTA^{4-}$ and $DTPA^{5-}$ derivatives and that a similar lengthening might even exist between the M^{III} ($M^{III} = La^{3+}$, Ce^{3+}) $DOTA^{4-}$ and $DTPA^{5-}$ derivatives in aqueous solution.

The different structures adopted in aqueous solution by the $[Gd(DOTA)(H_2O)]^{-}$, $[Eu(DTPA)(H_2O)]^{3-}$, $[Eu(DOTA)(H_2O)]^{2-}$, and $[Eu(ODDA)(H_2O)]$ complexes were found to be responsible for the shift in the water exchange mechanism from D to I_d, I, and I_a, respectively. Three reasons are proposed to explain why the Eu^{2+} poly(amino carboxylate) complexes feature water exchange rates 3 orders of magnitude higher than those of the corresponding Gd^{3+} complexes: first, a lower charge density on the Eu^{2+} metal ion; second, substantially longer $M-O_w$ distances for the Eu^{2+} ion; and third, a change in the water exchange mechanism from D ($DTPA^{5-}$, $DOTA^{4-}$) for Gd^{3+} to I_d ($DTPA^{5-}$), I ($DOTA^{4-}$), and I_a ($ODDA^{2-}$) for the Eu^{2+} complexes.

Acknowledgment. We thank S. Laus, F. Bouamrane, the LURE D21 beam line staff (R. Cortes, S. Bénazeth, and I. Ascone) for their technical collaboration. We also thank the Laboratoire pour l'Utilisation du Rayonnement Electromagnétique (LURE) for the beam time allocation and laboratory facilities. We finally acknowledge the Swiss National Science Foundation, the Latvian National Science Foundation, the COST actions D9 (Advanced Computational Chemistry of Increasingly Complex Systems), and D18 (Lanthanide Chemistry for Diagnosis and Therapy) for financial support.

Supporting Information Available: Results from the analyses with theoretical phases and amplitudes with all of the experimental details. XAFS experimental spectra after first-shell filtering of the Sr^{2+} and Eu^{2+} DOTA,$^{4-}$ $DTPA^{5-}$, and $ODDA^{2-}$ complexes in the solid state and in aqueous solution, together with the fitted spectra with theoretical phases and amplitudes. A comparison of the Eu L_3-edge XANES spectra of the Eu^{2+} DOTA,$^{4-}$ $DTPA^{5-}$, and $ODDA^{2-}$ complexes in the solid state and in solution and a comparison of the Sr K-edge XANES spectra of the Sr^{2+} DOTA,$^{4-}$ $DTPA^{5-}$, and $ODDA^{2-}$ complexes in the solid state and in solution. This material is available free of charge via the Internet at http://pubs.acs.org.

References and Notes

(1) *The Chemistry of Contrast Agents in Medical Magnetic Resonance Imaging*; Merbach, A. E., Toth, E., Eds.; Wiley & Sons: Chichester, U.K., 2001.

(2) Shannon, R. D. *Acta Crystallogr., Sect. A* **1976**, *32*, 751.

(3) Toth, E.; Helm, L.; Merbach, A. E. In *Topics in Current Chemistry;* Springer-Verlag: Berlin, 2002; Vol. 221.

(4) Toth, E.; Burai, L.; Merbach, A. E. *Coord. Chem. Rev.* **2001**, *216−217*, 363.

(5) McCoy, H. N. *J. Am. Chem. Soc.* **1936**, *58*, 1577.

(6) Johnson, D. A. *Adv. Inorg. Chem. Radiochem.* **1977**, *20*, 1.

(7) Mikheev, N. B.; Kamenskaya, A. N. *Coord. Chem. Rev.* **1991**, *109*, 1.

(8) Moreau, G.; Helm, L.; Purans, J.; Merbach, A. E. *J. Phys. Chem. A* **2002**, *106*, 3034.

(9) Seibig, S.; Toth, E.; Merbach, A. E. *J. Am. Chem. Soc.* **2000**, *122*, 5822.

(10) Burai, L.; Toth, E.; Seibig, S.; Scopelliti, R.; Merbach, A. E. *Chem.−Eur. J.* **2000**, *6*, 3761.

(11) Burai, L.; Toth, E.; Moreau, G.; Sour, A.; Scopelliti, R.; Merbach, A. E. *Chem. Eur. J.*, in press.

(12) Benazeth, S.; Purans, J.; Chalbot, M.-C.; Nguyen-van-Duong, M. K.; Nicolas, L.; Keller, F.; Gaudemer, A. *Inorg. Chem.* **1998**, *37*, 3667.

(13) Rehr, J. J.; Mustre de Leon, J.; Zabinsky, S. I.; Albers, R. C. *J. Am. Chem. Soc.* **1991**, *113*, 5135.

(14) Bunker, G. *Nucl. Instrum. Methods* **1983**, *207*, 437.

(15) Sayers, D. E.; Bunker, B. A. In *X-ray Absorption*; Koningsberger, D. C., Prins, R., Eds.; Chemical Analysis; Wiley & Sons: New York, 1988; Vol. 92, p 211.

(16) Crozier, E. D.; Rehr, J. J.; Ingalls, R. In *X-ray Absorption*; Koningsberger, D. C., Prins, R., Eds.; Chemical Analysis; Wiley & Sons: New York, 1988; Vol. 92, p 373.

(17) Harrowfield, J. M.; Kepert, D. L.; Patrick, J. M.; White, A. H. *Aust. J. Chem.* **1983**, *36*, 483.

(18) Besler, B. H.; Merz, K. M. J.; Kollman, P. A. *J. Comput. Chem.* **1990**, *11*, 431.

(19) Frisch, M. J.; Trucks, G. W.; Schlegel, H. B.; Scuseria, G. E.; Robb, M. A.; Cheeseman, J. R.; Zakrzewski, V. G.; Montgomery, J. A., Jr.; Stratmann, R. E.; Burant, J. C.; Dapprich, S.; Millam, J. M.; Daniels, A. D.; Kudin, K. N.; Strain, M. C.; Farkas, O.; Tomasi, J.; Barone, V.; Cossi, M.; Cammi, R.; Mennucci, B.; Pomelli, C.; Adamo, C.; Clifford, S.; Ochterski, J.; Petersson, G. A.; Ayala, P. Y.; Cui, Q.; Morokuma, K.; Malick, D. K.; Rabuck, A. D.; Raghavachari, K.; Foresman, J. B.; Cioslowski, J.; Ortiz, J. V.; Stefanov, B. B.; Liu, G.; Liashenko, A.; Piskorz, P.; Komaromi, I.; Gomperts, R.; Martin, R. L.; Fox, D. J.; Keith, T.; Al-Laham, M. A.; Peng, C. Y.; Nanayakkara, A.; Gonzalez, C.; Challacombe, M.; Gill, P. M. W.; Johnson, B. G.; Chen, W.; Wong, M. W.; Andres, J. L.; Head-Gordon, M.; Replogle, E. S.; Pople, J. A. *Gaussian 98*, revision A.5; Gaussian, Inc.: Pittsburgh, PA, 1998.

(20) Chang, C. A.; Francesconi, L. C.; Malley, M. F.; Kumar, K.; Gougoutas, J. Z.; Tweedle, M. F. *Inorg. Chem.* **1993**, *32*, 3501.

(21) Jin, T. Z.; Zhao, S. F.; Xu, G. X.; Han, Y. Z.; Shi, N. C.; Ma, Z. S. *Acta Chim. Sin. (Engl. Ed.)* **1991**, *49*, 569.
(22) Dolg, M.; Stoll, H.; Savin, A.; Preuss, H. *Theor. Chim. Acta* **1989**, *75*, 173.
(23) Portmann, S.; Lüthi, H. P. *Chimia* **2000**, *54*, 766.
(24) Villain, F.; Briois, V.; Castro, I.; Helary, C.; Verdaguer, M. *Anal. Chem.* **1993**, *65*, 2545.
(25) Binsted, N.; Strange, R. W.; Hasnain, S. S. *Biochemistry* **1992**, *31*, 12117.
(26) Agondanou, J.-H.; Spyroulias, G. A.; Purans, J.; Tsikalas, G.; Souleau, C.; Coutsolelos, A. G.; Benazeth, S. *Inorg. Chem.* **2001**, *40*, 6088.
(27) Kuzmin, A. *Physica B* **1995**, *208*−*209*, 175.
(28) Moreau, G.; Scopelliti, R.; Helm, L.; Purans, J.; Merbach, A. E. *J. Phys. Chem. A* **2002**, *106*, 9612.
(29) Rocca, F.; Kuzmin, A.; Purans, J.; Mariotto, G. *Phys. Rev. B* **1994**, *50*, 6662.
(30) Dalba, G.; Fornasini, P. *J. Synchrotron Radiat.* **1997**, *4*, 243.
(31) Bianconi, A. In *EXAFS and Near Edge Structure*; Bianconi, A., Incoccia, L., Stipcich, S., Eds.; Springer: Berlin, 1983; p 118.
(32) Teo, B. K. *EXAFS: Basic Principles and Data Analysis*; Springer-Verlag: Berlin, 1986.
(33) *X-ray Absorption Fine Structure*; Hasnain, S. S., Ed.; Ellis Horwood: New York, 1991; p 751.
(34) Starynowicz, P. *Polyedron* **1995**, *14*, 3573.
(35) Trunov, V. K.; Chubinidze, A. D.; Efremov, V. A.; Velikodni, Y. A. *Koord. Khim.* **1984**, *10*, 403.
(36) Woods, M.; Aime, S.; Botta, M.; Howard, J. A. K.; Moloney, J. M.; Navet, M.; Parker, D.; Port, M.; Rousseaux, O. *J. Am. Chem. Soc.* **2000**, *122*, 9781.
(37) Uggeri, F.; Aime, S.; Anelli, P. L.; Botta, M.; Brocchetta, M.; de Haen, C.; Ermondi, G.; Grandi, M.; Paoli, P. *Inorg. Chem.* **1995**, *34*, 633.
(38) Caulfield, T. J.; Guo, P.; Illig, C. R.; Kellar, K. E.; Liversidge, E.; Shen, J.; Wellons, J.; Ladd, D.; Peltier, N.; Toner, J. L. *Bioorg. Med. Chem. Lett.* **1995**, *5*, 1657.
(39) Kang, S. I.; Ranganathan, R. S.; Emswiler, J. E.; Kumar, K.; Gougoutas, J. Z.; Malley, M. F.; Tweedle, M. F. *Inorg. Chem.* **1993**, *32*, 2912.
(40) Kumar, K.; Chang, C. A.; Francesconi, L. C.; Dischino, D. D.; Malley, M. F.; Gougoutas, J. Z.; Tweedle, M. F. *Inorg. Chem.* **1994**, *33*, 3567.
(41) Aime, S.; Batsanov, A. S.; Botta, M.; Dickins, R. S.; Faulkner, S.; Foster, C. E.; Harrison, A.; Howard, J. A. K.; Moloney, J. M.; Norman, T. J.; Parker, D.; Royle, L.; Williams, J. A. G. *J. Chem. Soc., Dalton Trans.* **1997**, 3623.
(42) Aime, S.; Botta, M.; Fasano, M.; Marques, M. P. M.; Geraldes, C. F. G. C.; Pubanz, D.; Merbach, A. E. *Inorg. Chem.* **1997**, *36*, 2059.
(43) Dunand, F.; Aime, S.; Merbach, A. E. *J. Am. Chem. Soc.* **2000**, *122*, 1506.
(44) Dunand, F.; Dickins, R. S.; Parker, D.; Merbach, A. E. *Chem.—Eur. J.* **2001**, *7*, 5160.
(45) Micskei, K.; Helm, L.; Brucher, E.; Merbach, A. E. *Inorg. Chem.* **1993**, *32*, 3844.
(46) Powell, D. H.; Ni Dhubhghaill, O. M.; Pubanz, D.; Helm, L.; Lebedev, Y. S.; Schlaepfer, W.; Merbach, A. E. *J. Am. Chem. Soc.* **1996**, *118*, 9333.
(47) Pubanz, D.; Gonzalez, G.; Powell, D. H.; Merbach, A. E. *Inorg. Chem.* **1995**, *34*, 4447.
(48) Micskei, K.; Powell, D. H.; Helm, L.; Brucher, E.; Merbach, A. E. *Magn. Reson. Chem.* **1993**, *31*, 1011.